DLK inhibition has sex-specific effects on neuroprotection and locomotor recovery after spinal cord injury

John C. Aldrich[a,b], Samantha M. Alman[a,b], Sydney E. Lee[a,b], Ashley R. Scheinfeld[a,b], Chelsea C. Zhang[a,b], Averi L. Pike[c], Fiona C. Bremner[a,b], Olivia Calderon[d], Sunil Goodwani[d], William J. Ray[d], Andrew D. Gaudet[a,b,e*]

[a] Department of Psychology, College of Liberal Arts, University of Texas at Austin, Austin, TX 78712, USA
[b] Department of Neurology, Dell Medical School, University of Texas at Austin, Austin, TX 78712, USA
[c] Department of Molecular Biosciences, University of Texas at Austin, Austin, TX 78712, USA
[d] Belfer Neurodegeneration Consortium, Therapeutics Discovery Division, University of Texas MD Anderson Cancer Center, Houston, TX 77054, USA
[e] Interdisciplinary Neuroscience Program, University of Texas at Austin, Austin, TX 78712, USA

***Corresponding Author:**

Andrew Gaudet: andrew.gaudet@utexas.edu

Department of Psychology
University of Texas at Austin
108 E. Dean Keeton Street, Stop A8000, Seay Building, Room 4.208
Austin, TX 78712
USA

Tel: +1-512-471-1157
Fax: +1-512-471-6175
ORCID ID: 0000-0001-8828-1553

ABSTRACT

Spinal cord injury (SCI) causes devastating functional deficits, in part due to neuroinflammation, oxidative stress, and excitotoxicity that drive death of lesion-adjacent viable neurons. One signaling protein that promotes neuronal apoptosis and activates stress-responsive genes is dual leucine zipper kinase (DLK), which is a neuron-enriched kinase that responds to extracellular stress by activating the c-Jun N-terminal kinase (JNK) pathway. We hypothesized that SCI would robustly activate DLK signaling and that acute pharmacological inhibition of DLK would suppress JNK pathway activation, thereby enhancing neuroprotection and locomotor recovery in our mouse model of moderate contusion SCI. Using western blotting, we observed that SCI induced strong and sustained activation of the JNK pathway in the injured spinal cord starting at 4 hours post-injury through 7 days. Complementary analysis of single-nucleus RNA-seq revealed that DLK expression is highly enriched in neurons across all injury phases. Following SCI, neurons exhibited robust, time-dependent upregulation of multiple DLK-responsive transcripts, consistent with sustained pathway activation during the acute and subacute periods. Systemic treatment with the selective DLK inhibitor IACS'825 effectively suppressed intraspinal JUN activation in a dose-dependent manner. However, unexpectedly, DLK inhibition delayed functional recovery in male mice and expanded lesion volume by 71%, with no significant effect in females. These findings highlight the complex roles of DLK signaling after SCI, revealing a need to understand the sex-specific molecular mechanisms that modulate injury outcomes. Future studies should further optimize timing, location, and cellular targeting of DLK therapeutic strategies to improve neuroprotection and neurologic recovery after SCI.

INTRODUCTION

Spinal cord injury (SCI) causes loss of motor, sensory, and autonomic function, creating chronic locomotor deficits and neuropathic pain that can permanently burden affected individuals (Ahuja et al., 2017; Anjum et al., 2020). Following the initial mechanical insult, inflammation and excitotoxicity create a stressful microenvironment within the injured spinal cord that leads to the loss of otherwise viable neurons. This secondary damage limits the long-term potential for functional recovery (Gaudet & Fonken, 2018; Lukacova et al., 2021; Pang et al., 2022). Preventing secondary damage and neuronal loss during the early stages of injury remains a central goal of research involving rodent models of SCI, yet effective therapies that improve long-term outcomes remain elusive. As such, there is growing interest in targeting neuron-intrinsic pathways that regulate stress responses and determine cell survival after injury.

Dual leucine zipper kinase (DLK, encoded by *Map3k12*) is a critical neuron-intrinsic sensor of cellular stress, rapidly activated in response to axonal injury, metabolic stress, and extracellular signals such as inflammation and excitotoxicity (Pozniak et al., 2013; Shin, Ha, Kim, Cho, & DiAntonio, 2019; Tedeschi & Bradke, 2013; Watkins et al., 2013). Upon activation, DLK initiates signaling through the JNK (Jun N-terminal kinase) pathway, leading to phosphorylation of the transcription factor JUN and induction of transcriptional programs involved in stress mediation. While these programs can promote both regenerative and apoptotic processes, in most contexts sustained injury-induced DLK activation drives neuronal apoptosis and degeneration. In the adult central nervous system—where regenerative capacity is inherently limited—the consequences of modulating DLK signaling remain poorly understood. Although combined neuronal knockout of DLK and its closely related ortholog LZK (Leucine Zipper Kinase, *Map3k13*) can reduces axon regeneration and sprouting after hemisection SCI (Saikia et al., 2022), targeted pharmacological inhibition or selective modulation of DLK has not been evaluated after SCI. DLK inhibition improves neuronal survival and limits degeneration in models of glaucoma, amyotrophic lateral sclerosis, and Alzheimer's disease, highlighting its potential as a neuroprotective strategy following SCI (Le Pichon et al., 2017; Patel et al., 2015; Siu, Sengupta Ghosh, & Lewcock, 2018; Welsbie et al., 2013; Wlaschin et al., 2018).

Given DLK's central role in neuronal stress signaling, selective small molecule inhibitors targeting this kinase have been developed to enable neuron-specific modulation of the JNK pathway (Bu et al., 2023; Oetjen & Lemcke, 2016; Patel et al., 2015). IACS'825, a highly selective, brain-penetrant DLK inhibitor has demonstrated robust *in vivo* efficacy and therapeutic potential in models of peripheral neuropathy (Le et al., 2023; Ma et al., 2021). In this study, we evaluated the effects of DLK inhibition in a mouse model of moderate contusion SCI. We hypothesized that SCI would induce DLK signaling in the injured spinal cord and that acute pharmacological inhibition would enhance neuroprotection and promote locomotor recovery. Western blotting and single-nucleus RNA-Seq analyses confirmed that JUN and other DLK targets are strongly activated after SCI and remain elevated through the acute to subacute phase. Treatment with IACS'825 suppressed JUN activation in a dose-dependent manner. However, contrary to our hypothesis, DLK inhibition delayed locomotor recovery and

increased lesion size—effects that were restricted to male mice and suggest a previously unrecognized sex-specific consequence of targeting this pathway.

METHODS

Animals and housing

All housing, surgery, and postoperative care procedures were approved by The University of Texas at Austin Institutional Animal Care and Use Committee (Protocol AUP-2021-00171). Adult (12-16 weeks old) male and female C57BL/6J mice (Jackson Laboratory, Stock 000664) were housed in sex-matched pairs, provided standard chow and filtered tap water *ad libitum*, and maintained on a 12:12 light/dark cycle. Mice in all treatment groups were numbered randomly to ensure experimenters were blind to group assignments.

Surgeries and postoperative care

All surgeries were performed as previously described (Gaudet et al., 2016; Lee et al., 2023; Scheff, Rabchevsky, Fugaccia, Main, & Lumpp, 2003) between Zeitgeber time (ZT) 2–6. Mice were anesthetized with isoflurane inhalation anesthesia (1.5%; MWI Animal Health, Cat. 502017) and received prophylactic buprenorphine hydrochloride (0.075 mg/kg; MWI Animal Health, Cat. 060969) immediately prior to surgery. A dorsal T9 laminectomy was performed, with the periosteum but not the dura removed. Sham mice received no further injury. For SCI mice, a moderate contusion injury (65 kdyn, 0 s dwell) was delivered at T9 using the Infinite Horizon impactor (Precision Systems and Instrumentation). Incisions were closed using sutures and wound clips. Postoperative care included daily subcutaneous injections of Ringer's solution (2, 2, 1, 1, 1 mL on postoperative days 1–5) to prevent dehydration and manual bladder expression twice daily, which was reduced to once daily once bladder function returned. Mice were monitored at least once daily for signs of infection or abnormal recovery.

Drug formulation and delivery

IACS'825 was provided by the M.D. Anderson Belfer Neurodegeneration Consortium and is described previously (Le et al., 2023; Ma et al., 2021). For initial dose-response characterization, IACS'825 was formulated fresh in 0.5% (w/v) methylcellulose in water (10 mL/kg) and administered once by oral gavage 3 hours post-surgery at 3, 10, or 30 mg/kg. The compound was suspended in vehicle, vortexed, sonicated in a water bath (10 min and homogenized using a BioSpec Tissue-Tearor (5–7 min, half speed). Lower doses were prepared by diluting the 30 mg/kg formulation in 0.5% methylcellulose. Solutions were kept at room temperature with continuous mixing until dosing. Vehicle control mice received 0.5% methylcellulose alone.

For continual dosing, IACS'825 was prepared in a vehicle of polyethylene glycol 400 (PEG-400; MilliporeSigma) and polysorbate 80 (Tween-80; MilliporeSigma) in sterile water (40:10:50, v/v/v; 10 mL/kg) and administered intraperitoneally at 30 mg/kg beginning 3 h post-SCI and then at 2, 4, and 6 dpo (ZT2). The compound was dissolved in the PEG-400/Tween-80 mixture by vortexing (30 s, maximum speed) and sonicating in a water bath sonicator at room temperature (10–30 min) until fully dissolved. Sterile water was then added, and the solution was vortexed vigorously for 30–60 s before dosing. Vehicle control mice received PEG-400/Tween-80/sterile water alone.

Locomotor testing
Hindlimb motor function was assessed using the Basso Mouse Scale (BMS; Basso et al., 2006) prior to surgery and at 1, 4, 7, 10, 14, 21, and 28 days post-injury (dpo). Recovery was scored on the BMS scale of 0 (complete paralysis) to 9 (normal motor function) by two observers blinded to treatment conditions. For statistical analysis (see below) left and right hindlimb scores were included as a fixed effect; since there was no significant difference between sides ($F_{1,297} = 0.23$; $p = 0.632$), the average of both was used for visualization purposes. Final group sizes were 6 females and 5 males per treatment group.

Western blotting
Western blotting was performed as previously described (Goodwani et al., 2020). Briefly, mice were euthanized with Euthasol (200–270 mg/kg; Virbac AH, Inc), transcardially perfused with ice-cold PBS, and a 5 mm spinal cord segment centered at the T9 lesion epicenter was dissected and flash frozen on dry ice. Tissue was lysed in radioimmunoprecipitation assay (RIPA) buffer containing protease and phosphatase inhibitors, homogenized on ice, and centrifuged at 14,000 × *g* for 30 min at 4 °C. Protein concentrations were determined by DC Protein Assay, diluted in loading buffer with 2-mercaptoethanol, denatured, separated by SDS-PAGE, and transferred to nitrocellulose membranes. Membranes were blocked, incubated overnight at 4 °C with primary antibodies against phospho–c-Jun (pJUN; Abcam, ab32385; 1:100), c-Jun (Cell Signaling Technology, 9165; 1:250), phospho–MKK4 (pMAP2K4; Cell Signaling Technology, 9156; 1:100), and GAPDH (MilliporeSigma, MAB374; 1:5000), followed by IRDye-conjugated secondary antibodies (LI-COR Biosciences, 1:5000). Immunoreactive bands were visualized using an Odyssey CLx Imaging System (LI-COR Biosciences) and quantified with Image Studio software. Individual datapoints are plotted in each figure and n is provided in the figure caption.

Tissue collection and processing
Mice were euthanized via an intraperitoneal injection of Euthasol (200–270 mg/kg; Virbac AH, Inc.) followed by transcardial perfusion with cold 1× phosphate-buffered saline (PBS; pH 7.4) and 4% paraformaldehyde (PFA) in PBS. Spinal cords (5 mm segments including the injury epicenter and 2.5 mm rostral and caudal) were dissected and post-fixed overnight in cold 4% PFA before transfer to 30% sucrose the following day. Tissue was embedded in optimal cutting temperature (OCT; Fisherbrand) compound, flash frozen on dry ice, and sectioned at 12 µm on a cryostat. Serial cross sections were collected onto Superfrost Plus slides (Fisherbrand) and stored at –20 °C until use. Mice were randomized so that tissue collection, handling, and subsequent analysis were performed in a blinded manner.

Immunohistochemistry, imaging, and lesion analysis
Immunohistochemistry was performed as previously described (Aldrich et al., 2024; Gaudet et al., 2016). Briefly, slides were brought to room temperature, encircled with a hydrophobic barrier pen, washed in PBS, and blocked for 1 h at room temperature in 10% normal donkey serum (NDS) in PBS with 0.2% Triton X-100 (PBTx). Sections were incubated overnight at 4 °C with Rabbit anti-GFAP (1:500; Cell Signaling Technology,

3670) diluted in 10% NDS in PBTx. The following day, slides were washed, incubated for 2 h at room temperature with Donkey anti-Rabbit Alexa Fluor 488 or 568 (1:500; Thermo Fisher Scientific) and DAPI (1:10,000), washed again, mounted in Immu-Mount (Epredia), coverslipped, and sealed. Spinal cord sections were imaged on a Nikon Ni-E widefield epifluorescence microscope using the "acquire large image" function in Nikon Elements (AR 5.21.02) at the Center for Biomedical Research Support Microscopy and Flow Cytometry Facility at UT Austin (RRID:SCR_021756). Nine overlapping 10× fields were stitched to form each composite image. For each mouse, the epicenter section—defined as the section with the largest GFAP-negative lesion area—plus five rostral and five caudal sections spaced 200 µm apart were acquired. Lesion area and total cross-sectional area were quantified in ImageJ (v2.1.0; Fiji distribution) based on GFAP staining (Schindelin et al., 2012; Schneider, Rasband, & Eliceiri, 2012). Final group sizes were 5 females and 4 males per treatment group.

Single-nucleus RNA sequencing analysis

For snRNA-Seq analyses, we used data from the *Tabulae Paralytica* atlas (Gene Expression Omnibus, accession GSE234774) comprising uninjured mice and mice at 1, 4, 7, 14, 30, or 60 days after mid-thoracic (T10) crush spinal cord injury (Skinnider et al., 2024). For downstream analyses, we used the authors' quality-filtered dataset and cell type annotations, which were generated via iterative clustering with *Seura*t to assign cell types and subtypes based on established marker gene expression.

Processed count matrices, feature tables, and metadata were downloaded from GEO and assembled into a Seurat object using the *ReadMtx*, *read.delim*, and *CreateSeuratObject* functions in the *Seurat R* package (v5.3.0; Hao et al., 2024). To quantify expression of *Map3k12* (DLK) and *Map3k13* (LZK), we calculated the percentage of cells with ≥ 1 count for each gene within each layer (layer1) for all biological replicates, excluding categories with fewer than 25 cells per replicate. We also fit binomial generalized linear mixed models (GLMMs) using *lme4* (v1.1-37 ; Bates, Mächler, Bolker, & Walker, 2015) and *broom.mixed* (v0.2.9.6) for each layer and for all subtypes (layers 1–5), including a log10-transformed total count term to control for library size and replicate ID to account for between-sample variation. Counts were aggregated within each layer using *Seurat's AggregateExpression* function, and differential gene expression was tested with *DESeq2* (v1.42.1; Love, Huber, & Anders, 2014). For the time course, we used a likelihood ratio test (LRT) to identify genes whose expression varied across time points, and a Wald test to compare each time point to the uninjured condition for neurons only. For the 7 dpo analysis, we used a Wald test to compare gene expression between males and females for each layer. Uncorrected p-values from *DESeq2* were collected across all layers and cell types, and a global false discovery rate (FDR) adjustment was applied to obtain adjusted p-values (Benjamini & Hochberg, 1995).

Statistics, data analysis, and visualization

For western blot time course data, two-way ANOVAs (type III sum of squares) were performed for each target using the *Anova* function from the *car* package (v3.1-3; Fox & Weisberg, 2019), with group (sham, 4 h, 1 d, 7 d post-injury), sex, and their interaction as fixed effects, and blot number included as a covariate to control for variation across

different blots. *Post-hoc* comparisons were performed using estimated marginal means via the *emmeans* library (v1.11.1; Lenth, 2024) comparing each SCI timepoint to sham controls and adjusting p-values for multiple testing via the FDR method. For dose–response results, type III ANOVA was again used with dose (as a numeric variable), sex, and their interaction as fixed effects along with blot number as a covariate. *Post-hoc* contrasts were assessed using *emmeans* to compare each dose to the vehicle control.

For analysis of repeated measures data (BMS scores across multiple days and lesion size at serial tissue sections), we fit linear mixed-effects models using *lmerTest* (v3.1-3; Kuznetsova, Brockhoff, & Christensen, 2017), including mouse ID as a random effect. Upon detecting a significant *treatment x sex x dpo* interaction in the BMS data, BMS scores and lesion size were analyzed separately for males and females, with fixed effects including treatment, time (or section order), and their interactions; for BMS scores, foot was also included as a fixed effect. When significant interactions were detected, post-hoc contrasts were performed with *emmeans* using FDR correction. For lesion volume, we performed two-tailed Welch's t-tests to compare treatment groups within sex using the *t.test* function from the *stats* package (v4.3.2).

All data analysis and visualization were performed in *R* (v4.3.2; R Core Team, 2022) using *RStudio* (v2025.5.1.513; RStudio Team, 2020).Data wrangling was done primarily with *tidyverse* (v2.0.0), especially *dplyr* (v1.1.4). Figures were generated with *ggplot2* (v3.5.2) except for heatmaps, which were created with *ComplexHeatmap* (v2.18.0l; Gu, Eils, & Schlesner, 2016). Multi-panel figures were assembled using *cowplot* (v1.1.3), *ggpubr* (v0.6.0), *legendry* (v0.2.2), and *patchwork* (v1.3.0). Color palettes were optimized for color-blind accessibility with *scico* (v1.5.0) (Crameri, Shephard, & Heron, 2024). Additional tools included *ggrepel* (v0.9.6) for labeling volcano plots*, ggbeeswarm* (v0.7.2) for jitter plots, and *ggtext* (v0.1.2) for formatted text. Data import/export used *readr* (v2.1.5), *readxl* (v1.4.5), and *openxlsx* (v4.2.8). The *ragg* package (v1.4.0) was used for high-quality graphics rendering, and *conflicted* (v1.2.0) was used to manage function conflicts between packages.

RESULTS

SCI activates the DLK/JNK pathway in the lesion epicenter

DLK is a central mediator of neuronal stress signaling and is a promising therapeutic target in models of axonal injury and neurodegeneration (Patel et al., 2015; Tedeschi & Bradke, 2013). DLK activates downstream responses via the MAP2K4,7–JNK–JUN signaling axis (**Fig. 1A**), leading to transcriptional activation of stress response and apoptotic pathways. To assess pathway activation in our spinal cord injury (SCI) model, we performed moderate (65 kdyn) T9 contusion injuries in adult male and female C57BL/6 mice and collected epicenter tissue at 4 hours, 1 day, and 7 days post-injury. Western blotting was used to quantify phosphorylation of MAP2K4 and JUN, as well as total JUN expression levels, which are induced downstream of this pathway (**Fig. 1B–D**; **Fig. S1**).

Phosphorylated MAP2K4 (pMAP2K4) was elevated by 4 hours post-injury and peaked at ~2-fold above sham at 1 dpo ($p = 0.007$; **Fig. 1B**). Phospho-JUN increased similarly by 4 hours and peaked at ~6.8-fold above sham at 1 day ($p = 0.0003$), with elevated levels persisting through 7 days ($p = 0.028$; **Fig. 1C**). Total JUN protein also rose by 4 hours, peaked at 3-fold at 1 day, and remained elevated at 7 days ($p = 1.5 \times 10^{-5}$ and $p = 0.016$; **Fig. 1D**). There were no detectable main effects of sex ($F_{1,13} \leq 1.2$, $p \geq 0.29$) or sex × group interactions ($F_{1,13} \leq 0.21$, $p \geq 0.89$) for targets examined (**Table S1** & **S2**). Overall, these data show sustained activation of DLK/JNK signaling during the first week following SCI.

DLK expression is enriched in neurons across SCI timepoints

To evaluate the cell-type specificity of DLK expression in the spinal cord, we re-analyzed single-nucleus RNA-sequencing (snRNA-Seq) data from *Tabulae Paralytica* atlas which includes samples from the lesion epicenter at multiple timepoints following SCI, as well as uninjured controls (Skinnider et al., 2024). Expression of DLK (i.e., *Map3k12*) was generally low and sparse across all populations. To simplify interpretation and minimize variability across replicates, we grouped cells into four time bins—uninjured, acute (1–4 dpo), subacute (7–14 dpo), and chronic (30–60 dpo)—and calculated the proportion of cells with detectable *Map3k12* expression (>0 counts) within each major cell class. Neurons consistently showed the highest proportion of DLK-expressing cells across all phases (**Fig. 2A**).

To formally test whether DLK expression is preferentially associated with neurons, we used a binomial generalized linear model to estimate the likelihood of *Map3k12* detection within each major class relative to all others. Neurons were the only population with consistently elevated odds of DLK expression across all injury phases (odds ratio ≥ 1.6, FDR-adjusted $p \leq 2 \times 10^{-27}$). In contrast, other classes—including oligodendrocytes, immune cells, and astroependymal populations—generally exhibited depletion of DLK, with only transient enrichment observed at isolated timepoints (**Fig. 2B, Table S3**).

Next, we applied the same modeling approach to all annotated cell subtypes in the dataset, including granular distinctions among neuronal, immune, vascular, and glial populations (**Fig. 2C, Table S4**). Subtypes were pooled across timepoints to reduce dimensionality and increase the representation of rarer cell populations. Of the 47

neuronal subtypes examined, 26 showed significantly elevated likelihood of DLK expression (odds ratio ≥ 1.14, FDR-adjusted p ≤ 0.034), and none were significantly depleted. In contrast, only five non-neuronal subtypes showed significant enrichment, including two oligodendrocyte progenitor populations (odds ratio ≥ 1.27, FDR-adjusted p ≤ 0.030). A complementary pseudobulk RNA-Seq analysis using a similar one-versus-all approach mirrored these results, with *Map3k12* significantly upregulated in 73% of neuronal subtypes along with the same two oligodendrocyte populations (**Fig. S2**, **Table S5**). Together, these findings indicate that DLK is predominantly expressed in neurons, supporting its relevance as a neuron-intrinsic target for modulating stress responses and promoting neuroprotection following SCI.

SCI induces expression of DLK-responsive genes

To assess DLK pathway activation in neurons after SCI, we performed pseudobulk differential expression analysis using aggregated snRNA-Seq data from all spinal cord neurons. Counts were summed per replicate and timepoint, and gene-level changes relative to uninjured controls were quantified using *DESeq2* (Love et al., 2014). From this broader dataset, we evaluated a curated set of DLK-responsive genes, including canonical DLK/JNK targets and transcripts previously identified as DLK-dependent following optic nerve crush (Watkins et al., 2013)**.**

Of the 381 DLK-associated genes detected in the neuronal pseudobulk dataset, 58.3% showed significant changes over time (FDR-adjusted p < 0.05 based on likelihood ratio testing; **Table S6, Fig. 3A**). These findings are consistent with our western blot results from bulk spinal cord tissue (**Fig. 1B–D**) and indicate that neurons mount a robust, time-dependent transcriptional response involving established DLK/JNK targets after SCI.

Expression patterns among these DLK-associated genes grouped into four clusters, with representative examples shown in **Fig. 3B**. Cluster 1 genes, such as *Nts*—involved in synaptic signaling—were higher at baseline and were suppressed post-injury, with varying degrees of return toward pre-injury levels by 30–60 days. Cluster 2 genes showed a brief spike at 4 days post-injury after early suppression; this included *Hrk*, a pro-apoptotic factor, which increased ~2.6-fold at 4 dpo ($p = 2 \times 10^{-9}$). Cluster 3, the largest group, consisted of transcripts that peaked at 4 dpo and returned to baseline by 7 days. These included well-known regeneration-associated genes *Sox11*, *Gadd45a*, and *Ecel1*. Cluster 4 genes—including *Atf3*, *Clic4,* Ddit3 (i.e., CHOP, an ER stress response gene)—rose at 1 dpo, peaked at 4 dpo, and remained elevated through at least 30 days. *Atf3* was among the most strongly induced, with >13-fold upregulation at 4 dpo ($p = 3.2 \times 10^{-15}$).

Together, these findings demonstrate that SCI causes neurons to upregulate multiple DLK-responsive transcripts, with coordinated transcriptional activation evident throughout the acute post-injury phase (1–7 dpo).

Pharmacological DLK inhibition suppresses JUN activation following SCI

Given the sustained activation of DLK signaling observed in neurons during the acute phase of SCI, we next tested whether pharmacological DLK inhibition could suppress downstream JUN activation *in vivo*. In a dose-response study, adult mice received oral IACS'825 at doses that achieve low, moderate, and high CNS target engagement (3,

10, or 30 mg/kg) or vehicle control 3 hours after moderate T9 contusion SCI. Spinal cord tissue was collected 24 hours later for western blot analysis of phospho-JUN and total JUN.

IACS'825 treatment reduced SCI epicenter phospho-JUN levels in a dose-dependent manner ($F_{3,25}$ = 10.7, p = 6.3 x 10^{-4}; **Fig. 4A, B**, **Fig. S3, Table S7**). All three DLK inhibitor doses reduced epicenter pJUN relative to vehicle, with the 30 mg/kg group showing the largest effect (effect size = –6.5; p = 1 x 10^{-4}, **Table S8**). Similar results were observed for total JUN (**Fig. 4C**), with 30 mg/kg IACS'825 most potently decreasing epicenter JUN (ANOVA $F_{3,25}$ = 15.7, p = 7.8 x 10^{-6}; *post hoc* effect size = –2.9; p = 8.5 x 10^{-6}).

To facilitate repeated dosing across the full acute phase (1–7 dpo), we reformulated IACS'825 for intraperitoneal (i.p.) injection and adopted an every-other-day schedule. This route was selected to minimize stress associated with repeated oral gavage (Balcombe, Barnard, & Sandusky, 2004; Larcombe, Wang, Phan, Berry, & Noble, 2019; Vanhecke, Bugada, Steiner, Polić, & Buch, 2024). To confirm efficacy, mice received a single 30 mg/kg i.p. dose 3 hours post-injury, and tissue was collected 48 hours later. As with oral delivery, i.p. DLK inhibitor reduced epicenter pJUN levels relative to vehicle (ANOVA $F_{2,18}$ = 32, p = 1.2 x 10^{-6}; *post hoc* p = 1.1 x 10^{-4}; **Fig. 4D, Fig. S4, Table S9** & **S10**). These results suggest that DLK inhibition via IACS'825 is an effective means of suppressing JNK pathway activation after SCI.

DLK inhibition delays locomotor recovery in male mice after SCI

To assess the functional consequences of DLK inhibition, mice received IACS'825 (30 mg/kg) or vehicle starting 3 hours post-SCI, with subsequent injections every 48 hours through 6 days post-injury (**Fig. 5A**). Locomotor function was evaluated using the Basso Mouse Scale (BMS) at 1, 4, 7, 10, 14, 21, and 28 dpo.

DLK inhibition selectively impaired locomotor recovery in male mice during the early post-injury period. Longitudinal analysis of BMS scores revealed a significant treatment × day × sex interaction ($F_{7,297}$ = 2.1, p = 0.042; **Fig. 5B, Table S11**). When stratified by sex, IACS'825-treated males exhibited significantly lower BMS scores at 10, 14, and 21 dpo, with the largest effect observed at 10 dpo (estimate = –2.2, p = 4.7 x 10^{-6}; **Fig. 5C, Table S12**). At this timepoint, vehicle-treated males averaged 4.6 ± 0.4—consistent with the onset of occasional plantar stepping—while drug-treated males averaged 2.4 ± 0.3, indicating a delay in recovery. By 10 dpo, 4 of 5 vehicle-treated males exhibited plantar stepping, compared to only 1 of 5 in the IACS'825 group. Despite these early differences, males from both treatment groups reached similar endpoints by 28 dpo, averaging a score of ~6, which corresponds to frequent to consistent plantar stepping with at least some forelimb–hindlimb coordination (**Fig. 5D**). In contrast, female mice showed no significant difference in recovery between treatment groups at any timepoint (**Fig. 5E, F**). These results indicate that DLK inhibition via systemic IACS'825 treatment does not enhance locomotor recovery after SCI, and instead transiently delays locomotor recovery in male mice.

DLK inhibition increases lesion size in male mice after SCI

To evaluate the histological impact of DLK inhibition, we analyzed serial 12 µm cryosections spanning the lesion epicenter using fluorescence immunohistochemistry.

Lesion and spared tissue areas were quantified using widefield fluorescence microscopy of GFAP-immunolabeled sections (**Fig. 6A**). The lesion was defined as the central GFAP-negative region, and spared tissue was calculated as the remaining GFAP-positive area expressed as a percentage of the total cross-sectional area.

Consistent with our BMS results, DLK inhibition exacerbates tissue damage in male mice following SCI. When analyzing both sexes (**Fig. S5, Table S13**), we observed a treatment × sex interaction for both lesion area ($F_{1,14} = 5.7$, $p = 0.03$) and percent spared tissue ($F_{1,14} = 5.3$, $p = 0.04$), prompting follow-up analysis stratified by sex. In male mice, IACS'825 treatment increased lesion area relative to vehicle-treated controls (**Fig. 6B**; LMM main effect of treatment: $F_{1,6.5} = 18.3$, $p = 0.004$). Lesion volumes interpolated from these measurements showed a 0.2 mm^3 increase in the IACS'825 treatment group—equivalent to a 71% increase relative to vehicle (unpaired t-test: $t_{3.8} = 5.04$, $p = 0.008$; **Fig. 6C**). Quantification of percent spared tissue mirrored these results ($F_{1,6} = 14$, $p = 0.009$; **Fig. S6A, B**).

No differences between vehicle or IACS'825 treatment were observed in female SCI mice for lesion area ($F_{1,8} = 0.11$, $p = 0.75$; **Fig. 6D, Table S13**), lesion volume ($t_8 = -0.45$, $p = 0.67$; **Fig. 6E**), or spared tissue ($F_{1,8} < 0.01$, $p = 0.9$; **Fig. S4C, D**). These findings align with the locomotor recovery data, indicating that systemic DLK inhibition fails to promote tissue preservation after SCI and may worsen outcomes in males. Together, the data show that while IACS'825 effectively targets the DLK pathway, it does not confer neuroprotection or functional benefit following spinal cord injury.

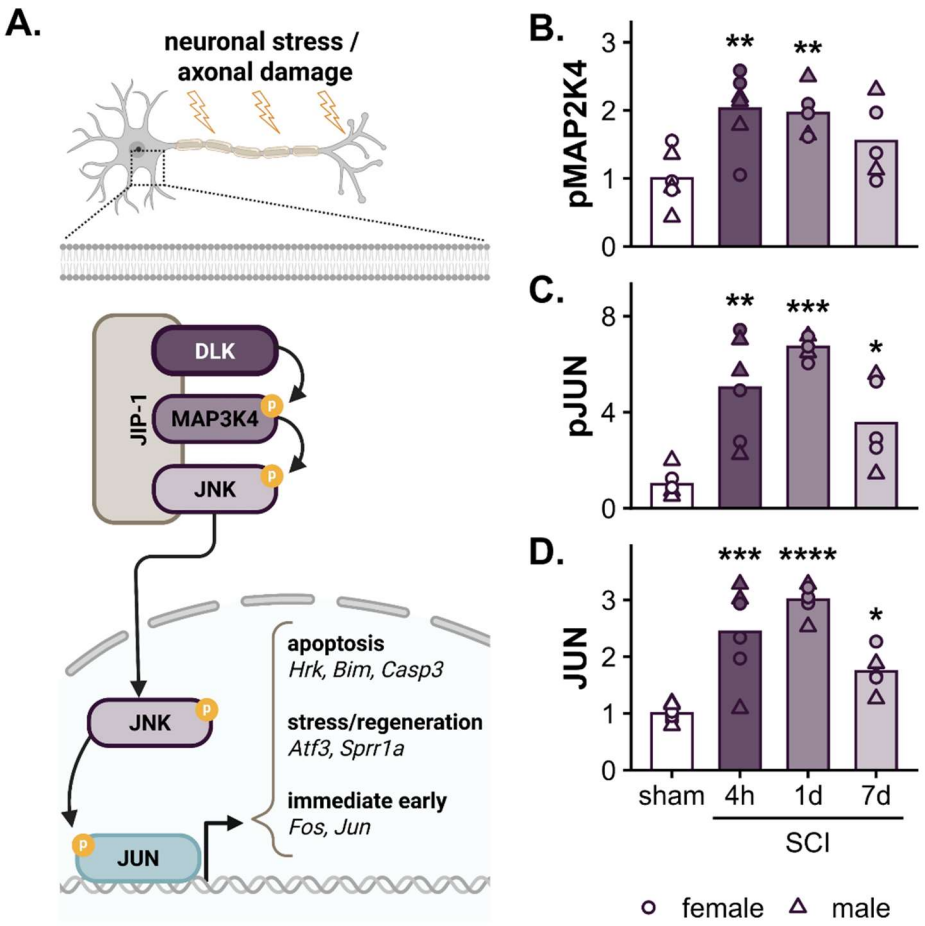

Figure 1: SCI activates DLK/JNK signaling in the lesion epicenter.
(A) Schematic of the DLK signaling cascade. Extracellular stress activates DLK, which phosphorylates MAP2K4, leading to phosphorylation of JNK. JNK translocates to the nucleus and activates the transcription factor JUN. **(B)** Western blot quantification of phospho-MAP2K4 (pMAP2K4), phospho-JUN (pJUN), and total JUN protein levels in the lesion epicenter at 4 hours, 24 hours, and 7 days post-SCI, compared to sham. GAPDH was used as a loading control, and values are expressed relative to sham. Each point represents an individual mouse (n = 2-3/sex/group): females (circles), males (triangles). Asterisks indicate significant post-hoc comparisons to sham following a significant group effect in two-way ANOVA (**Table S1** & **S2**): *$p < 0.05$), **$p < 0.01$, ***$p < 0.001$, ****$p < 0.0001$. Pathway diagram created in BioRender (2025) https://BioRender.com/r0daq7w.

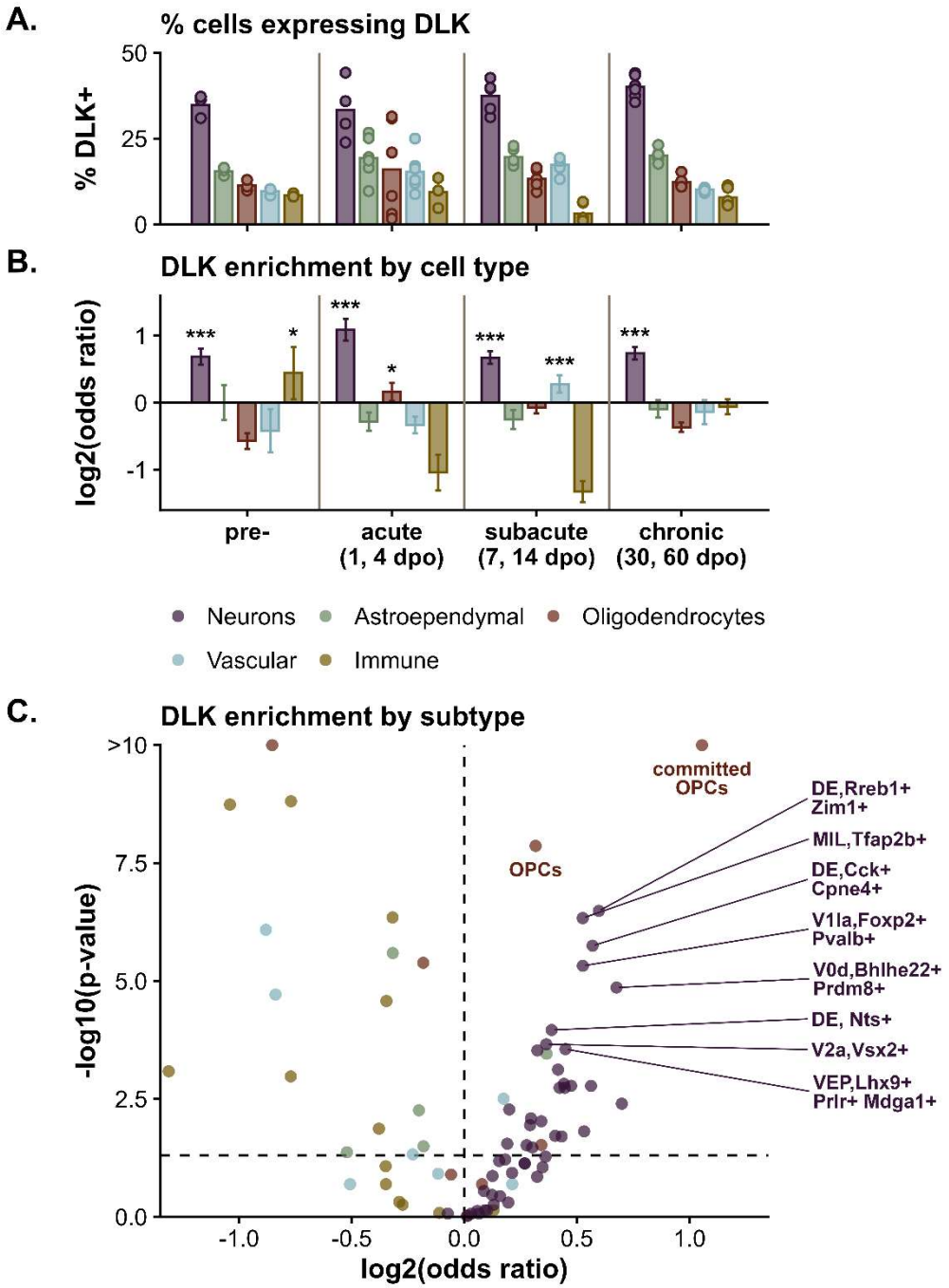

Figure 2: DLK expression is enriched in spinal neurons before and after SCI.
(A) Percentage of DLK-expressing cells (*Map3k12* > 0) across major cell types and SCI phases, derived from published single-nucleus RNA-Seq data. Each point represents the average per biological replicate; n = 2-3 female mice per time. Timepoints are grouped into uninjured, acute (1–4 days post-injury), subacute (7–14 days), and chronic (30–60 days). **(B)** Cell type–specific enrichment of DLK expression, estimated using a binomial generalized linear model. Plotted are $\log_2$ odds ratios (OR) with 95% confidence intervals. Asterisks indicate statistically significant enrichment compared to all other cell types (*$p < 0.05$, **$p < 0.01$, ***$p < 0.001$, ****$p < 0.0001$). **(C)** Subtype-level enrichment of DLK expression using the same modeling approach, aggregated across timepoints. Each point represents a distinct cell subtype; x-axis shows $-\log_{10}$(FDR-adjusted *p*-value), y-axis shows $\log_2$ odds ratio. The ten most significantly enriched subtypes (positive $\log_2$ OR) are labeled: DE (dorsal excitatory), MIL (medial excitatory, lateral), V1 (ventral inhibitory interneurons), V2 (ventral excitatory interneurons), V0 (ventral commissural interneurons), VEP (ventral excitatory projection neurons); OPC (oligodendrocyte precursor cells).

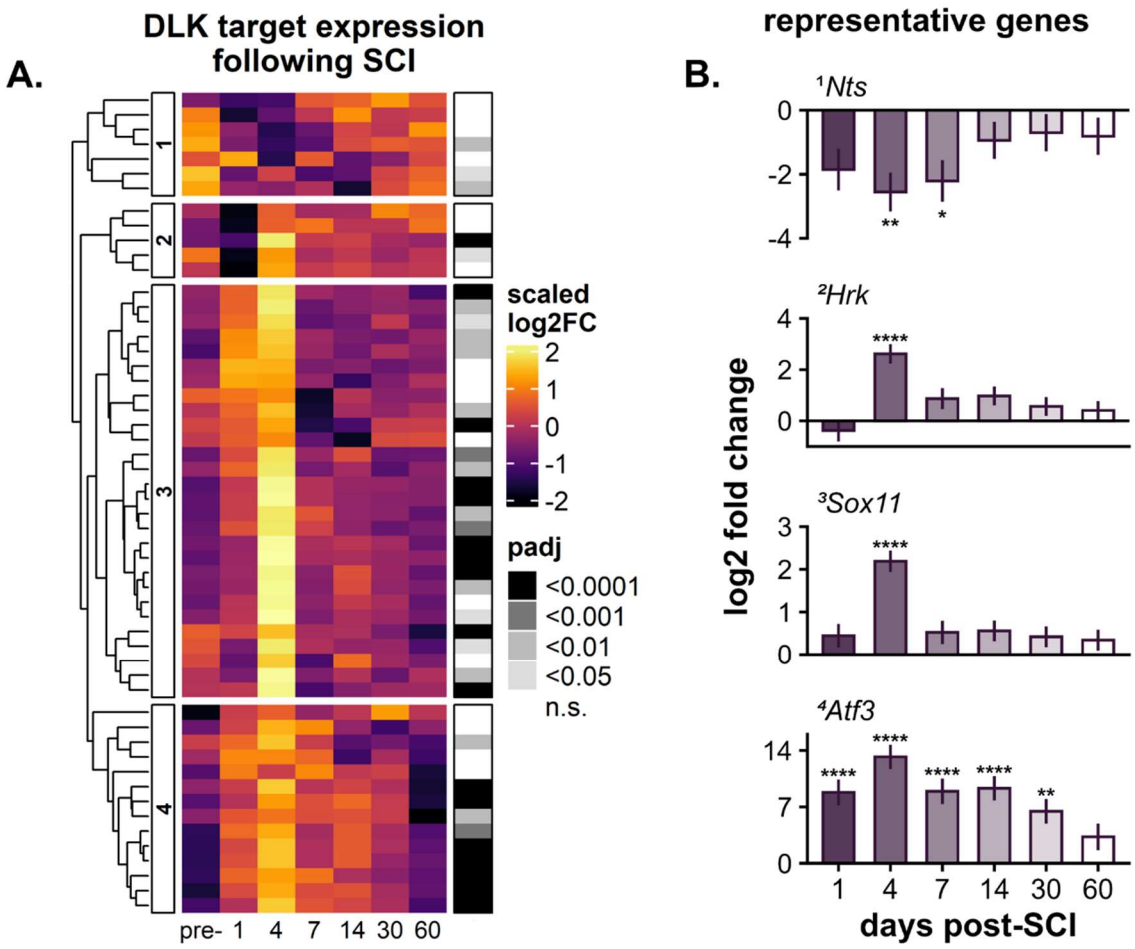

Figure 3: DLK-responsive genes are transcriptionally induced in neurons after SCI. (A) Pseudobulk differential expression analysis of DLK-associated genes in spinal cord neurons across timepoints following SCI. Rows represent individual genes and columns represent discrete timepoints from uninjured through 60 days post-injury. Color reflects row-scaled (z-score) $\log_2$ fold change values calculated from pairwise comparisons to uninjured controls. Genes are grouped by hierarchical clustering using Euclidean distance and complete linkage. Cluster identities are shown numerically to the left, and FDR-adjusted p-values from likelihood ratio testing are indicated by grayscale. **(B)** Expression profiles of representative DLK-responsive genes from each cluster identified in **(A)**, showing $\log_2$ fold change (mean ± standard error) relative to uninjured controls at each timepoint. Asterisks indicate significant differences compared to uninjured (*$p < 0.05$, **$p < 0.01$, ***$p < 0.001$, ****$p < 0.0001$; FDR-adjusted).

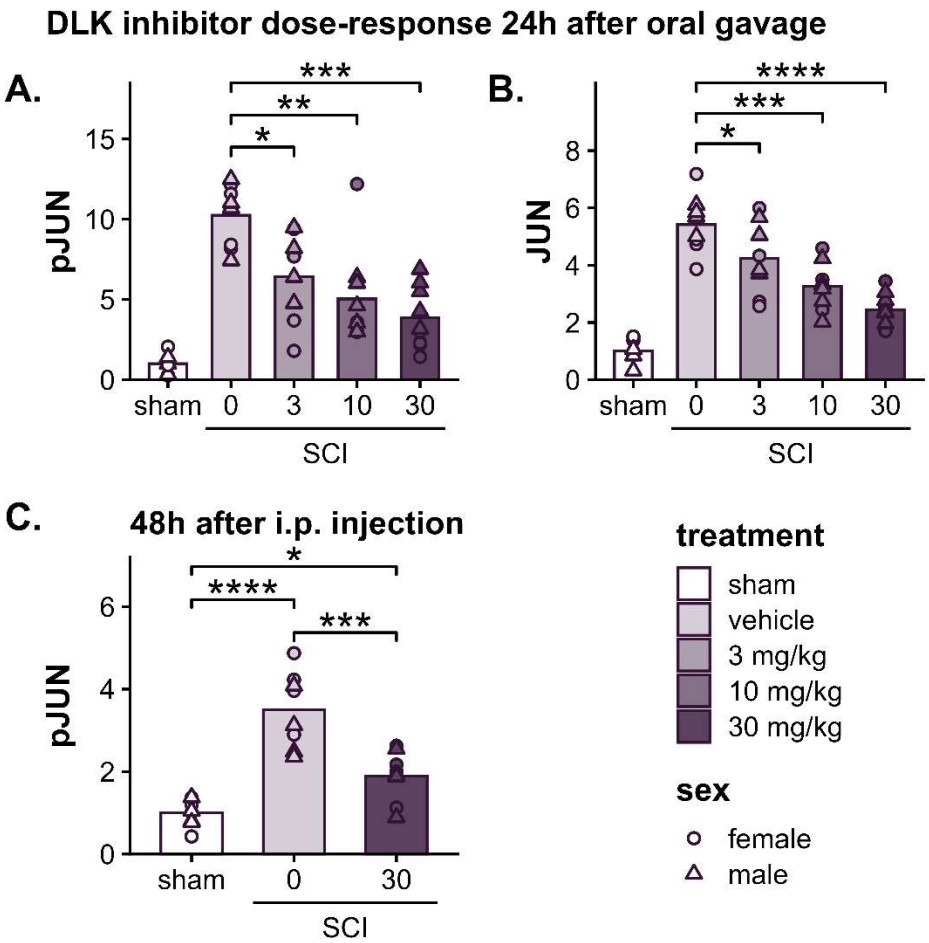

Figure 4: Pharmacological DLK inhibition suppresses JUN phosphorylation after SCI. (A) Phospho-JUN (pJUN) levels in spinal cord epicenter tissue 24 hours after SCI and oral administration of DLK inhibitor IACS'825 (3, 10, or 30 mg/kg) or vehicle. IACS'825 treatment produced a dose-dependent reduction in pJUN compared to vehicle. **(B)** Total JUN levels from the same samples, showing a similar dose-dependent decrease. **(C)** pJUN levels 48 hours after SCI and a single intraperitoneal (i.p.) injection of IACS'825 (30 mg/kg) or vehicle. All values are normalized to GAPDH and expressed relative to sham. Circles represent females, triangles represent males (3–4 mice per sex per group). Asterisks indicate significant *post-hoc* comparisons (*$p < 0.05$, **$p < 0.01$, ***$p < 0.001$, ****$p < 0.0001$) following a significant group effect in two-way ANOVA.

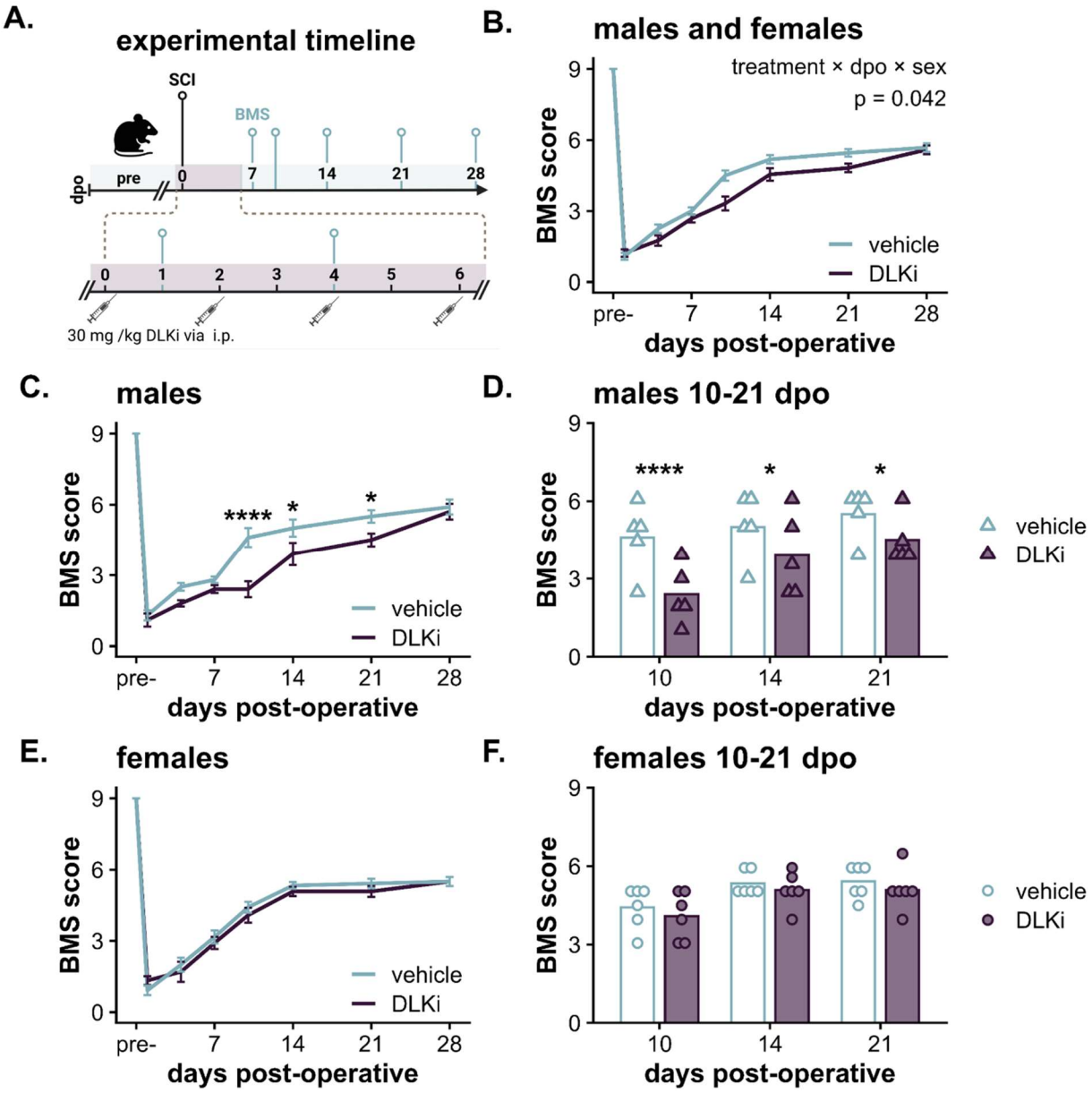

Figure 5: Systemic DLK inhibition after SCI impairs locomotor recovery in males but has no significant effect in females. (A) Experimental timeline. Mice received DLK inhibitor IACS'825 (DLKi; 30 mg/kg) or vehicle beginning 3 hours post-injury, with repeat dosing every 48 hours through 6 days post-SCI. BMS scoring was performed at the indicated timepoints, and tissue was collected at 28 days post-injury. **(B)** DLKi treatment does not improve BMS scores when analyzing males and females combined (vehicle vs. DLKi; females: n = 6 per group, males: n = 5 per group). Values reflect mean of left and right hindlimb scores ± SEM. A significant treatment × day × sex interaction was detected via linear mixed-effects model. **(C)** In males, IACS'825 treatment led to significantly lower BMS scores at 10–21 days post-injury. **(D)** Individual male scores during this interval. **(E)** DLKi treatment had no significant effect on BMS scores in female mice overall or at specific timepoints **(F)**. Asterisks indicate significant *post-hoc* comparisons between treatment groups (FDR-adjusted). (*$p < 0.05$, **$p < 0.01$, ***$p < 0.001$, ****$p < 0.0001$). Timeline Created in BioRender. (2025) https://BioRender.com/9528xxc.

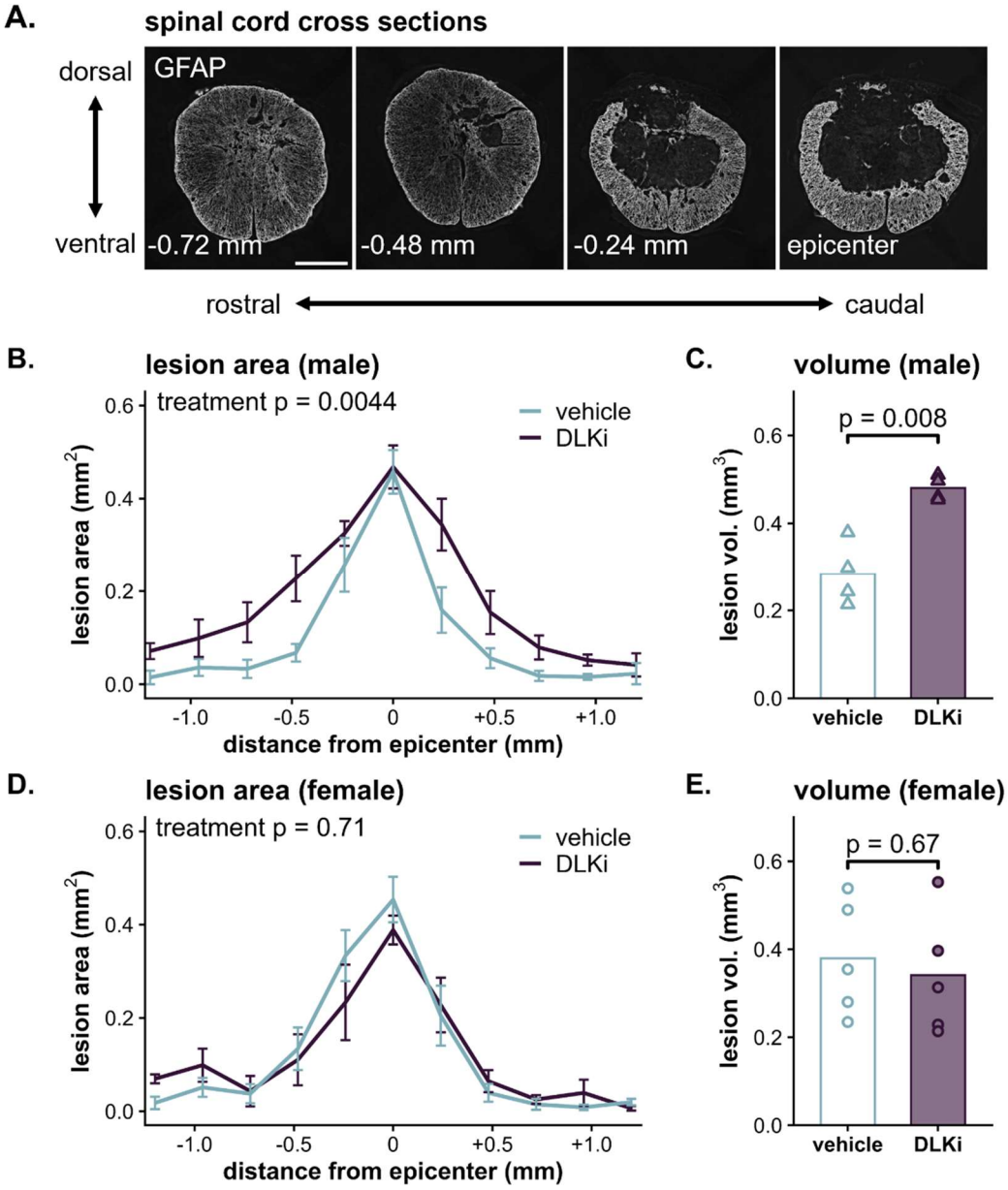

Figure 6: Systemic DLK inhibitor delivery has sex-dependent effects on neuroprotection after SCI. (A) GFAP-immunolabeled spinal cord cross sections 28 days after dorsal midline contusion SCI. Lesion area was defined as the central GFAP-negative region, and spared tissue was calculated as the remaining GFAP-positive area. Scale bar indicates 0.4 mm. (**B**) IACS'825 (DLKi) increased lesion area in males across serial sections ±1.3 mm from the epicenter. (**C**) Lesion volume, estimated by interpolating area measurements, was greater in treated males. (**D**) DLKi had no significant effect on lesion area in females. (**E**) Lesion volume in females was similar between groups. females: *n* = 5 per group, males: *n* = 4 per group. P-values in panels **B** and **D** reflect main effects of treatment from linear mixed-effects models (treatment × position), while those in **C** and **E** are from unpaired t-tests comparing total lesion volume. Error bars represent SEM. See **Figure S4** for spared tissue quantification.

DISCUSSION

DLK is an evolutionarily conserved neuronal stress sensor studied across various model systems (e.g., *Drosophila*, *C. elegans*, and mammals) in diverse injury and disease contexts (Le Pichon et al., 2017; Tedeschi & Bradke, 2013; Xiong et al., 2010; Yan, Wu, Chisholm, & Jin, 2009). Despite its therapeutic potential, DLK remains relatively uncharacterized in the adult spinal cord, and its activation dynamics after SCI have not been well defined. DLK regulates neuronal stress and apoptosis primarily through the JNK pathway (Ghosh et al., 2011; Miller et al., 2009). As such, we found that contusion SCI induces robust phosphorylation of the JNK targets MAP2K4 and JUN in the epicenter throughout the acute-to-subacute post-injury phase. snRNA-Seq confirmed that DLK enrichment in spinal cord neurons and showed that SCI induces downstream transcriptional targets over a similar timeframe. We hypothesized that acute inhibition of DLK via IACS'825 would enhance neuroprotection and improve locomotor recovery after SCI. Although IACS'825 effectively reduced post-SCI JUN activation, it failed to improve functional outcomes and instead led to worse recovery in male mice. These results demonstrate that DLK is a viable pharmacological target for modulating JNK signaling after SCI, but that broad systemic DLK inhibition has sex-specific effects and is unlikely to support functional recovery.

Phosphorylation of DLK targets MAP2K4 and JUN increases rapidly by 4 hours post-SCI and remains elevated through 7 days (**Fig. 1**), mirroring DLK pathway activation in the optic nerve following both direct and indirect injury (Huntwork-Rodriguez et al., 2013; Watkins et al., 2013; Welsbie et al., 2019; Wong & Benowitz, 2022). Unlike DLK (**Fig. 2**), JUN is broadly expressed across neuronal and non-neuronal populations and can be activated by several upstream kinases. Nevertheless, studies using global DLK knockout in optic nerve injury models show that the characteristic injury-induced phosphorylation of JUN is almost completely lost without DLK, indicating that in CNS trauma contexts JUN activation is largely dependent on DLK signaling. (Le Pichon et al., 2017; Watkins et al., 2013). In the spinal cord, DLK is highly enriched in neurons, and pharmacological inhibition with IACS'825 markedly reduces pJUN after SCI (**Fig. 4**), suggesting that DLK signaling drives SCI-induced JNK pathway activation.

DLK activation triggers a transcriptional program that coordinates neuronal stress responses, apoptosis, and regenerative growth, largely via JUN-dependent regulation of downstream targets (Bu et al., 2023; Tedeschi & Bradke, 2013). In the ONC model, Watkins et al. identified a set of DLK-dependent genes whose injury-induced expression was abolished or attenuated in DLK knockout mice (Watkins et al., 2013). Using a previously published snRNA-Seq dataset, we found that many of these same genes—including *Atf3, Sox11*, and the pro-apoptotic factors *Hrk and Ddit3* (aka *CHOP*)—are induced in neurons after SCI (**Fig. 3**). Additionally, several canonical DLK pathway components absent from the Watkins list (e.g., *Jun* and other AP-1 transcription factors *Fos*, and *Fosl1*) were also induced in SCI epicenter. Together, these findings indicate that SCI engages a DLK-dependent transcriptional network closely paralleling that seen in the optic nerve, encompassing both stress-adaptive and pro-apoptotic elements.

In many models of neuronal injury and neurodegeneration, DLK loss-of-function or pharmacological inhibition confers neuroprotection, including paradigms such as

optic nerve injury, excitotoxicity, and tauopathy (Le Pichon et al., 2017; Pozniak et al., 2013; Welsbie et al., 2013) DLK also plays a critical role in neural development, regulating axon growth, neuronal migration, programmed apoptosis, and axon degeneration during circuit refinement and maturation (Ghosh et al., 2011; Hammarlund, Nix, Hauth, Jorgensen, & Bastiani, 2009; Miller et al., 2009; Tedeschi & Bradke, 2013; Yan et al., 2009). Other work has shown that DLK/JNK signaling is an key regulator of axonal regeneration, with injury-induced stress responses triggering transcriptional programs that can drive both axon growth and degeneration depending on context (Itoh, Horiuchi, Bannerman, Pleasure, & Itoh, 2009; Jin & Zheng, 2019; Shin et al., 2019). This dual capacity suggests that the impact of DLK inhibition likely varies with injury type, timing, and the relative contribution of protective versus regenerative responses.

Direct investigation of DLK in SCI remains limited. To date, the only *in vivo* study found that neuronal DLK/LZK double knockout reduced corticospinal tract axon regeneration in a *Pten*$^{-/-}$ background and suppressed spontaneous sprouting in wild-type mice, 18 weeks after dorsal hemisection SCI (Saikia et al., 2022). These effects were absent when either kinase was deleted alone, suggesting functional redundancy in the ability of DLK and LZK to enhance axon plasticity. Based on this and broader evidence that DLK can drive both degeneration and regeneration, we hypothesized that acute-to-subacute inhibition—when the post-SCI environment is most stressful—would suppress early maladaptive stress responses while sparing later regenerative processes. In our model, treatment with the DLK inhibitor IACS'825 during this early window reduced JUN phosphorylation (**Fig. 4**) but did not improve locomotor recovery (**Fig. 5**) or neuroprotection (**Fig. 6**).

This unexpected outcome may reflect opposing effects of DLK inhibition—limiting apoptosis but also constraining stress-adaptive and repair pathways—that offset each other's impact on functional recovery even at the acute-to-subacute timepoint. Our transcriptomic analysis supports this possibility: SCI induces both pro-apoptotic (e.g., *Hrk, Ddit3*) and stress-adaptive (e.g., *Atf3, Sox11*) DLK-dependent gene expression in spinal neurons (**Fig. 3**), suggesting that DLK activation engages parallel programs with potentially opposing functional consequences. Although axon plasticity is minimal in the injured adult spinal cord, many regeneration-associated factors are also linked to stress adaptation and may contribute to neuronal survival or repair (Mahar & Cavalli, 2018). Acute DLK inhibition with IACS'825 reduced JUN phosphorylation but may have simultaneously suppressed these protective responses, contributing to the absence of functional improvement. Importantly, our findings should not be taken to imply that all DLK inhibition is inherently detrimental. Rather, they highlight the limitations of broad kinase inhibition in this context. Recent work has shown that disrupting DLK's axonal localization can reduce pro-degenerative signaling while preserving beneficial transcriptional outputs (Zhang et al., 2025), suggesting that more targeted strategies may better dissociate these dual aspects of DLK function.

Notably, IACS'825 treatment led to worse locomotor recovery and lesion expansion in males, suggesting that the detrimental consequences of pathway suppression outweighed any potential benefits in this group (**Fig. 5, 6**). Although our western blot analyses were not specifically designed to assess sex differences (e.g., only 3–4 animals per sex per group were used), they revealed no obvious differences in

DLK/JNK activation post-SCI or in sensitivity to IACS'825 (**Fig. 1, 4**). This suggests that any sex differences in DLK/JNK signaling are either modest in magnitude or obscured by the cellular heterogeneity of bulk tissue preparations. Given the limited attention to sex as a variable in SCI research (Lee et al., 2023; Stewart et al., 2020), few datasets directly compare male and female responses. The *Tabulae Paralytica* single-cell atlas (Skinnider et al., 2024) is a notable exception, but still only includes a single male–female comparison at 7 dpo. Overall, the authors report very few sex differences in cell-type proportions, transcriptional programs, or neurological outcomes, noting that sex accounted for the least variance among all comparisons (e.g., age, injury model, severity, treatment, timepoint). Upon revisiting this dataset to specifically evaluate DLK/JNK pathway components, we unexpectedly found that DLK alone (i.e., *Map3k12*) is significantly upregulated in male microglia relative to females ($\log_2$ fold change = 5.7, $p = 0.006$) (**Fig. S7, Table S14**). This raises the possibility that non-neuronal DLK contributes to differential sensitivity between sexes. Astrocyte-specific deletion of LZK causes lesion expansion after SCI (Chen et al., 2018), providing a plausible precedent for DLK-family kinases influencing recovery through non-neuronal mechanisms. More definitive insights into neuronal and non-neuronal DLK function after SCI will require further studies using temporally and cell type–specific genetic approaches. The unexpected, male-specific effects observed here suggest that sex may critically shape the outcomes of DLK-targeted interventions and should be considered an essential variable in any future mechanistic and translational work.

CONCLUSION

Our study established that the validated DLK inhibitor IACS'825 reduced phosphorylation of targets including JUN in SCI lesion epicenter and that DLK is enriched in neurons within the spinal cord. Despite the promising spatiotemporal distribution of DLK and the effectiveness of the inhibitor, systemic delivery of the DLK inhibitor had no significant benefit on neuroprotection or locomotor recovery – systemic DLK inhibitor worsened neuroprotection and delayed locomotor recovery in males, but not females. Overall, the anatomical and functional effects of IACS'825 were minimal or negative, which contradicts our original hypothesis. Future studies should extend these findings by exploring the spatiotemporal effects of DLK inhibition – e.g., by refining timing, cellular specificity, or lesion-relative location of DLK inhibition. Another effective approach may involve targeting signaling mediators upstream or downstream of DLK, which may provide more precise modulation of specific cells or unidirectional tuning of a crucial process (e.g., cell survival or axon plasticity).

Our results highlight that the DLK pathway has an important role in regulating recovery after SCI, and in a sex-specific manner. Future research will help crystallize our understanding of the role of the DLK pathway after CNS injury. Ultimately, unravelling the intricacies of DLK signaling could lead to new neuroprotective therapies that improve recovery after SCI.

ACKNOWLEDGEMENTS
We thank the Animal Resources Center (ARC) husbandry staff at the Health Discovery Building for excellent animal care as well as the Center for Biomedical Research Support Microscopy and Flow Cytometry Facility at UT Austin (RRID:SCR_021756). Funding for this work was provided by the Belfer Neurodegeneration Consortium as well as the National Institute of Neurological Disorders And Stroke of the National Institutes of Health under Award Number R01NS131806 (ADG). The content is solely the responsibility of the authors and does not necessarily represent the official views of the National Institutes of Health.

WORKS CITED

Ahuja, C. S., Wilson, J. R., Nori, S., Kotter, M. R. N., Druschel, C., Curt, A., & Fehlings, M. G. (2017). Traumatic spinal cord injury. *Nature Reviews. Disease Primers*, *3*, 17018. doi: 10.1038/nrdp.2017.18

Aldrich, J. C., Scheinfeld, A. R., Lee, S. E., Dusenbery, K. J., Mahach, K. M., Van de Veire, B. C., … Gaudet, A. D. (2024). Effects of dim light at night in C57BL/6 J mice on recovery after spinal cord injury. *Experimental Neurology*, *375*, 114725. doi: 10.1016/j.expneurol.2024.114725

Anjum, A., Yazid, M. D., Fauzi Daud, M., Idris, J., Ng, A. M. H., Selvi Naicker, A., … Lokanathan, Y. (2020). Spinal Cord Injury: Pathophysiology, Multimolecular Interactions, and Underlying Recovery Mechanisms. *International Journal of Molecular Sciences*, *21*(20), 7533. doi: 10.3390/ijms21207533

Balcombe, J. P., Barnard, N. D., & Sandusky, C. (2004). Laboratory routines cause animal stress. *Contemporary Topics in Laboratory Animal Science*, *43*(6), 42–51.

Basso, D. M., Fisher, L. C., Anderson, A. J., Jakeman, L. B., McTigue, D. M., & Popovich, P. G. (2006). Basso Mouse Scale for locomotion detects differences in recovery after spinal cord injury in five common mouse strains. *Journal of Neurotrauma*, *23*(5), 635–659. doi: 10.1089/neu.2006.23.635

Bates, D., Mächler, M., Bolker, B., & Walker, S. (2015). Fitting Linear Mixed-Effects Models Using lme4. *Journal of Statistical Software*, *67*(1), 1–48. doi: 10.18637/jss.v067.i01

Benjamini, Y., & Hochberg, Y. (1995). Controlling the False Discovery Rate: A Practical and Powerful Approach to Multiple Testing. *Journal of the Royal Statistical*

Society: Series B (Methodological), *57*(1), 289–300. doi: 10.1111/j.2517-6161.1995.tb02031.x

Bu, H., Li, Z., Lu, Y., Zhuang, Z., Zhen, Y., & Zhang, L. (2023). Deciphering the multifunctional role of dual leucine zipper kinase (DLK) and its therapeutic potential in disease. *European Journal of Medicinal Chemistry*, *255*, 115404. doi: 10.1016/j.ejmech.2023.115404

Chen, M., Geoffroy, C. G., Meves, J. M., Narang, A., Li, Y., Nguyen, M. T., … Zheng, B. (2018). Leucine Zipper-Bearing Kinase Is a Critical Regulator of Astrocyte Reactivity in the Adult Mammalian CNS. *Cell Reports*, *22*(13), 3587–3597. doi: 10.1016/j.celrep.2018.02.102

Crameri, F., Shephard, G. E., & Heron, P. J. (2024). Choosing Suitable Color Palettes for Accessible and Accurate Science Figures. *Current Protocols*, *4*(8), e1126. doi: 10.1002/cpz1.1126

Fox, J., & Weisberg, S. (2019). *An R Companion to Applied Regression* (Third). Thousand Oaks CA: Sage. Retrieved from https://www.john-fox.ca/Companion/

Gaudet, A. D., & Fonken, L. K. (2018). Glial Cells Shape Pathology and Repair After Spinal Cord Injury. *Neurotherapeutics : The Journal of the American Society for Experimental NeuroTherapeutics*, *15*(3), 554–577. doi: 10.1007/s13311-018-0630-7

Gaudet, A. D., Mandrekar-Colucci, S., Hall, J. C. E., Sweet, D. R., Schmitt, P. J., Xu, X., … Popovich, P. G. (2016). miR-155 Deletion in Mice Overcomes Neuron-Intrinsic and Neuron-Extrinsic Barriers to Spinal Cord Repair. *The Journal of*

Neuroscience : The Official Journal of the Society for Neuroscience, *36*(32), 8516–8532. doi: 10.1523/JNEUROSCI.0735-16.2016

Ghosh, A. S., Wang, B., Pozniak, C. D., Chen, M., Watts, R. J., & Lewcock, J. W. (2011). DLK induces developmental neuronal degeneration via selective regulation of proapoptotic JNK activity. *The Journal of Cell Biology*, *194*(5), 751–764. doi: 10.1083/jcb.201103153

Goodwani, S., Fernandez, C., Acton, P. J., Buggia-Prevot, V., McReynolds, M. L., Ma, J., … Ray, W. J. (2020). Dual Leucine Zipper Kinase Is Constitutively Active in the Adult Mouse Brain and Has Both Stress-Induced and Homeostatic Functions. *International Journal of Molecular Sciences*, *21*(14), 4849. doi: 10.3390/ijms21144849

Gu, Z., Eils, R., & Schlesner, M. (2016). Complex heatmaps reveal patterns and correlations in multidimensional genomic data. *Bioinformatics*, *32*(18), 2847–2849. doi: 10.1093/bioinformatics/btw313

Hammarlund, M., Nix, P., Hauth, L., Jorgensen, E. M., & Bastiani, M. (2009). Axon Regeneration Requires a Conserved MAP Kinase Pathway. *Science*, *323*(5915), 802–806. doi: 10.1126/science.1165527

Hao, Y., Stuart, T., Kowalski, M. H., Choudhary, S., Hoffman, P., Hartman, A., … Satija, R. (2024). Dictionary learning for integrative, multimodal and scalable single-cell analysis. *Nature Biotechnology*, *42*(2), 293–304. doi: 10.1038/s41587-023-01767-y

Huntwork-Rodriguez, S., Wang, B., Watkins, T., Ghosh, A. S., Pozniak, C. D., Bustos, D., … Lewcock, J. W. (2013). JNK-mediated phosphorylation of DLK suppresses

its ubiquitination to promote neuronal apoptosis. *Journal of Cell Biology*, *202*(5), 747–763. doi: 10.1083/jcb.201303066

Itoh, A., Horiuchi, M., Bannerman, P., Pleasure, D., & Itoh, T. (2009). Impaired regenerative response of primary sensory neurons in ZPK/DLK gene-trap mice. *Biochemical and Biophysical Research Communications*, *383*(2), 258–262. doi: 10.1016/j.bbrc.2009.04.009

Jin, Y., & Zheng, B. (2019). Multitasking: Dual Leucine Zipper-Bearing Kinases in Neuronal Development and Stress Management. *Annual Review of Cell and Developmental Biology*, *35*, 501–521. doi: 10.1146/annurev-cellbio-100617-062644

Kuznetsova, A., Brockhoff, P. B., & Christensen, R. H. B. (2017). lmerTest Package: Tests in Linear Mixed Effects Models. *Journal of Statistical Software*, *82*(13), 1–26. doi: 10.18637/jss.v082.i13

Larcombe, A. N., Wang, K. C. W., Phan, J. A., Berry, L. J., & Noble, P. B. (2019). Confounding Effects of Gavage in Mice: Impaired Respiratory Structure and Function. *American Journal of Respiratory Cell and Molecular Biology*, *61*(6), 791–794. doi: 10.1165/rcmb.2019-0242LE

Le, K., Soth, M. J., Cross, J. B., Liu, G., Ray, W. J., Ma, J., … Jones, P. (2023). Discovery of IACS-52825, a Potent and Selective DLK Inhibitor for Treatment of Chemotherapy-Induced Peripheral Neuropathy. *Journal of Medicinal Chemistry*, *66*(14), 9954–9971. doi: 10.1021/acs.jmedchem.3c00788

Le Pichon, C. E., Meilandt, W. J., Dominguez, S., Solanoy, H., Lin, H., Ngu, H., … Lewcock, J. W. (2017). Loss of dual leucine zipper kinase signaling is protective

in animal models of neurodegenerative disease. *Science Translational Medicine*, *9*(403), eaag0394. doi: 10.1126/scitranslmed.aag0394

Lee, S. E., Greenough, E. K., Oancea, P., Scheinfeld, A. R., Douglas, A. M., & Gaudet, A. D. (2023). Sex Differences in Pain: Spinal Cord Injury in Female and Male Mice Elicits Behaviors Related to Neuropathic Pain. *Journal of Neurotrauma*. doi: 10.1089/neu.2022.0482

Lenth, R. V. (2024). *emmeans: Estimated Marginal Means, aka Least-Squares Means*. Retrieved from https://CRAN.R-project.org/package=emmeans

Love, M. I., Huber, W., & Anders, S. (2014). Moderated estimation of fold change and dispersion for RNA-seq data with DESeq2. *Genome Biology*, *15*(12), 550. doi: 10.1186/s13059-014-0550-8

Lukacova, N., Kisucka, A., Kiss Bimbova, K., Bacova, M., Ileninova, M., Kuruc, T., & Galik, J. (2021). Glial-Neuronal Interactions in Pathogenesis and Treatment of Spinal Cord Injury. *International Journal of Molecular Sciences*, *22*(24), 13577. doi: 10.3390/ijms222413577

Ma, J., Goodwani, S., Acton, P. J., Buggia-Prevot, V., Kesler, S. R., Jamal, I., … Heijnen, C. J. (2021). Inhibition of dual leucine zipper kinase prevents chemotherapy-induced peripheral neuropathy and cognitive impairments. *Pain*, *162*(10), 2599–2612. doi: 10.1097/j.pain.0000000000002256

Mahar, M., & Cavalli, V. (2018). Intrinsic mechanisms of neuronal axon regeneration. *Nature Reviews. Neuroscience*, *19*(6), 323–337. doi: 10.1038/s41583-018-0001-8

Miller, B. R., Press, C., Daniels, R. W., Sasaki, Y., Milbrandt, J., & DiAntonio, A. (2009). A dual leucine kinase–dependent axon self-destruction program promotes Wallerian degeneration. *Nature Neuroscience*, *12*(4), 387–389. doi: 10.1038/nn.2290

Oetjen, E., & Lemcke, T. (2016). Dual leucine zipper kinase (MAP3K12) modulators: A patent review (2010-2015). *Expert Opinion on Therapeutic Patents*, *26*(5), 607–616. doi: 10.1517/13543776.2016.1170810

Pang, Q.-M., Chen, S.-Y., Xu, Q.-J., Zhang, M., Liang, D.-F., Fu, S.-P., … Zhang, T. (2022). Effects of astrocytes and microglia on neuroinflammation after spinal cord injury and related immunomodulatory strategies. *International Immunopharmacology*, *108*, 108754. doi: 10.1016/j.intimp.2022.108754

Patel, S., Cohen, F., Dean, B. J., De La Torre, K., Deshmukh, G., Estrada, A. A., … Siu, M. (2015). Discovery of dual leucine zipper kinase (DLK, MAP3K12) inhibitors with activity in neurodegeneration models. *Journal of Medicinal Chemistry*, *58*(1), 401–418. doi: 10.1021/jm5013984

Pozniak, C. D., Sengupta Ghosh, A., Gogineni, A., Hanson, J. E., Lee, S.-H., Larson, J. L., … Lewcock, J. W. (2013). Dual leucine zipper kinase is required for excitotoxicity-induced neuronal degeneration. *The Journal of Experimental Medicine*, *210*(12), 2553–2567. doi: 10.1084/jem.20122832

R Core Team. (2022). *R: A Language and Environment for Statistical Computing*. Vienna, Austria: R Foundation for Statistical Computing. Retrieved from https://www.R-project.org/

RStudio Team. (2020). *RStudio: Integrated Development Environment for R*. Boston, MA: RStudio, PBC. Retrieved from http://www.rstudio.com/

Saikia, J. M., Chavez-Martinez, C. L., Kim, N. D., Allibhoy, S., Kim, H. J., Simonyan, L., … Zheng, B. (2022). A Critical Role for DLK and LZK in Axonal Repair in the Mammalian Spinal Cord. *The Journal of Neuroscience*, *42*(18), 3716–3732. doi: 10.1523/JNEUROSCI.2495-21.2022

Scheff, S. W., Rabchevsky, A. G., Fugaccia, I., Main, J. A., & Lumpp, J. E. J. (2003). Experimental modeling of spinal cord injury: Characterization of a force-defined injury device. *Journal of Neurotrauma*, *20*(2), 179–193. doi: 10.1089/08977150360547099

Schindelin, J., Arganda-Carreras, I., Frise, E., Kaynig, V., Longair, M., Pietzsch, T., … Cardona, A. (2012). Fiji: An open-source platform for biological-image analysis. *Nature Methods*, *9*(7), 676–682. doi: 10.1038/nmeth.2019

Schneider, C. A., Rasband, W. S., & Eliceiri, K. W. (2012). NIH Image to ImageJ: 25 years of image analysis. *Nature Methods*, *9*(7), 671–675. doi: 10.1038/nmeth.2089

Shin, J. E., Ha, H., Kim, Y. K., Cho, Y., & DiAntonio, A. (2019). DLK regulates a distinctive transcriptional regeneration program after peripheral nerve injury. *Neurobiology of Disease*, *127*, 178–192. doi: 10.1016/j.nbd.2019.02.001

Siu, M., Sengupta Ghosh, A., & Lewcock, J. W. (2018). Dual Leucine Zipper Kinase Inhibitors for the Treatment of Neurodegeneration. *Journal of Medicinal Chemistry*, *61*(18), 8078–8087. doi: 10.1021/acs.jmedchem.8b00370

Skinnider, M. A., Gautier, M., Teo, A. Y. Y., Kathe, C., Hutson, T. H., Laskaratos, A., … Courtine, G. (2024). Single-cell and spatial atlases of spinal cord injury in the Tabulae Paralytica. *Nature*, *631*(8019), 150–163. doi: 10.1038/s41586-024-07504-y

Stewart, A. N., MacLean, S. M., Stromberg, A. J., Whelan, J. P., Bailey, W. M., Gensel, J. C., & Wilson, M. E. (2020). Considerations for Studying Sex as a Biological Variable in Spinal Cord Injury. *Frontiers in Neurology*, *11*, 802. doi: 10.3389/fneur.2020.00802

Tedeschi, A., & Bradke, F. (2013). The DLK signalling pathway—A double-edged sword in neural development and regeneration. *EMBO Reports*, *14*(7), 605–614. doi: 10.1038/embor.2013.64

Vanhecke, D., Bugada, V., Steiner, R., Polić, B., & Buch, T. (2024). Refined tamoxifen administration in mice by encouraging voluntary consumption of palatable formulations. *Lab Animal*, *53*(8), 205–214. doi: 10.1038/s41684-024-01409-z

Watkins, T. A., Wang, B., Huntwork-Rodriguez, S., Yang, J., Jiang, Z., Eastham-Anderson, J., … Lewcock, J. W. (2013). DLK initiates a transcriptional program that couples apoptotic and regenerative responses to axonal injury. *Proceedings of the National Academy of Sciences of the United States of America*, *110*(10), 4039–4044. doi: 10.1073/pnas.1211074110

Welsbie, D. S., Yang, Z., Ge, Y., Mitchell, K. L., Zhou, X., Martin, S. E., … Zack, D. J. (2013). Functional genomic screening identifies dual leucine zipper kinase as a key mediator of retinal ganglion cell death. *Proceedings of the National Academy*

of Sciences of the United States of America, *110*(10), 4045–4050. doi: 10.1073/pnas.1211284110

Welsbie, D. S., Ziogas, N. K., Xu, L., Kim, B.-J., Ge, Y., Patel, A. K., … Koliatsos, V. E. (2019). Targeted disruption of dual leucine zipper kinase and leucine zipper kinase promotes neuronal survival in a model of diffuse traumatic brain injury. *Molecular Neurodegeneration*, *14*, 44. doi: 10.1186/s13024-019-0345-1

Wlaschin, J. J., Gluski, J. M., Nguyen, E., Silberberg, H., Thompson, J. H., Chesler, A. T., & Le Pichon, C. E. (2018). Dual leucine zipper kinase is required for mechanical allodynia and microgliosis after nerve injury. *eLife*, *7*, e33910. doi: 10.7554/eLife.33910

Wong, K. A., & Benowitz, L. I. (2022). Retinal Ganglion Cell Survival and Axon Regeneration after Optic Nerve Injury: Role of Inflammation and Other Factors. *International Journal of Molecular Sciences*, *23*(17), 10179. doi: 10.3390/ijms231710179

Xiong, X., Wang, X., Ewanek, R., Bhat, P., Diantonio, A., & Collins, C. A. (2010). Protein turnover of the Wallenda/DLK kinase regulates a retrograde response to axonal injury. *The Journal of Cell Biology*, *191*(1), 211–223. doi: 10.1083/jcb.201006039

Yan, D., Wu, Z., Chisholm, A. D., & Jin, Y. (2009). The DLK-1 Kinase Promotes mRNA Stability and Local Translation in *C. elegans* Synapses and Axon Regeneration. *Cell*, *138*(5), 1005–1018. doi: 10.1016/j.cell.2009.06.023

Zhang, X., Jeong, H., Niu, J., Holland, S. M., Rotanz, B. N., Gordon, J., … Thomas, G. M. (2025). Inhibiting acute, axonal DLK palmitoylation is neuroprotective and

avoids deleterious effects of cell-wide DLK inhibition. *Nature Communications*, *16*(1), 3031. doi: 10.1038/s41467-025-58036-6